Geotechnical Characterisation of Krishna Godavari Basin Sediments, Offshore Eastern India

T. M. Chang, X. Long, R. K. Ghanekar, S. Gamidi, A. Srivastava, R. Gunasekharan, P. Lakshminarayana, and S. Namburi

1 Introduction

A recent offshore geotechnical site investigation was carried out offshore India to evaluate the nature and mechanical properties of the soil to aid the design and future installation of subsea structures for a future development in the Krishna Godavari (KG) Basin, Bay of Bengal. This paper presents the key results and findings of the site investigation and subsequent comprehensive onshore laboratory testing and interpretation.

2 Geological Setting

The study area is located in the Krishna Godavari (KG) Basin off the east coast of India, which is within the eastern extended margin of India's peninsular stable continental region (SCR). The NNW-SSE-oriented Pranhita-Godavari Graben (PGG) or Godavari Rift is to the north of the study area and terminates at a NE-SW trending extended crustal terrane that forms the KG basin. The area is characterised by low rates of seismic activity. The Indian eastern continental margin within 500 km of

T. M. Chang (✉)
Fugro, Perth, WA, Australia
e-mail: t.chang@fugro.com

X. Long
Fugro, Houston, TX, USA

R. K. Ghanekar · S. Gamidi · A. Srivastava
Institute of Engineering and Ocean Technology, Navi Mumbai, Maharashtra, India

R. Gunasekharan · P. Lakshminarayana · S. Namburi
Oil and Natural Gas Corporation, East Offshore Asset, Kakinada, Andhra Pradesh, India

S. Haldar et al. (eds.), *Advances in Offshore Geotechnics*, Lecture Notes in Civil Engineering 92, https://doi.org/10.1007/978-981-15-6832-9_8

the site has seen only moderate magnitude earthquakes (Mw < 6) and low levels of seismic activity.

The submarine physiography offshore the Godavari Delta is subdivided into four major provinces: Shelf and Shelf Break, Slope, Toe-Thrust and Anticline, and Lower Slope. The Shelf and Shelf Break Province, as well as the upper slope within the Slope Province, are considered very dynamic areas due to the proximity of the Godavari River and Delta. The Godavari River is a monsoon-driven system and exhibits a very high sedimentation rate. This river has one of the largest sediment loads in India and is also considered one of the most turbid rivers. Subsidence onshore is comparable to that observed in other large rivers, such as the Nile or Yangtze; however, it is important to note that hundreds of dams have been constructed on the river over the past four decades, which has decreased the sediment discharge to the delta. Based on the analysis of satellite imagery and onshore coring data by Rao et al. (2015), there has been considerable coastal erosion of the Godavari Delta during the past four decades. Monsoon, cyclone/typhoon, and tsunami events have all affected the area in the recent past.

The site traverses a wide range of geologic features and conditions that are prevalent within each of the physiographic provinces. Water depths within the study area ranged between approximately 13 and 1559 m. The study area seafloor is generally characterised by the following types of features: sediment pathways, minor channels, moderate seafloor amplitudes, seafloor expression of blocky mass transport deposit, slumps, pathway margin mass movement, undulating seafloor, area of failures related to subsurface gas front, sediment wave areas, seafloor scarps, erosional scars, gullies, scoured irregular seafloor, seafloor and near seafloor fault scarps (normal and reverse), pockmark clusters, seafloor hydrate mounds, mud volcanoes, and elongated depressions. Several man-made features were also present in the area, consisting of drag scars, well mud splays, existing wells, possible wellheads and seafloor debris.

3 Summary of Fieldwork

The site investigation fieldwork was carried out from an 83 m, dynamic positioning (DP) Class 2 dedicated geotechnical drilling vessel capable of working in both downhole drilling and seabed modes in water depths up to 3000 m.

The investigation comprised offshore geotechnical and geological data acquisition through seabed and downhole mode sampling and in situ testing techniques. The drilling method consisted of a straight flush rotary system. Drilling was performed through a centre moonpool using a top drive power swivel with 5½″ standard drill pipes. Sampling was conducted through the open centre bit. Seawater was used to clean and stabilise the borehole when drilling in cohesive layers, while a mixture of bentonite or barite and drill water was used to flush or clean the hole.

For the seabed mode sampling, box corer (BC) and large gravity piston corer (LGPC) were deployed from an A-frame. Seabed mode piezocone penetrometer tests (PCPT), T-bar tests (TBT) and cyclic T-bar tests (CTBT) were conducted.

The soil samples from downhole mode were recovered by wire line push (WIP) or piston sampling (PIS) techniques either by using thin-walled tubes (76 mm OD, 72 mm ID) or thick-walled tubes (80 mm OD, 72 mm ID). Very soft to soft surficial clays were sampled using thin-walled tubes, fitted with 3 m PVC sample liner with 70 mm OD and 67 mm ID. The downhole PCPTs were performed using a 10 cm^2 base area, 60° cone with a 150 cm^2 cylindrical sleeve.

4 Summary of Laboratory Test Programme

A comprehensive soil testing programme was formulated to evaluate pertinent soil indices and engineering properties and was conducted in two phases; offshore laboratory tests performed on-board and onshore laboratory tests in several soil laboratories.

The offshore soil tests were performed concurrently with the drilling operations and were performed either while the sample was still inside the sample tube, or immediately after extrusion. Test types include laboratory (miniature) vane (intact and residual), unit weight determination, water contents and unconsolidated undrained (UU) triaxial compression (intact and remoulded).

After reviewing the field test results, an extensive onshore laboratory (static and cyclic) test programme was performed to characterise the sediments found across the study site. A study into the effect of strain rate on the monotonic shear strength was also included as part of the cyclic/dynamic test programme. The laboratory testing programme included monotonic and cyclic simple shear tests, monotonic and cyclic triaxial tests, bender element and resonant column tests. X-ray scans were also performed to ensure the best available samples were selected for strength testing.

The principal objectives of the laboratory test programme were to allow development of a site-wide monotonic undrained strength model, a strain rate effect model, a generalised cyclic undrained strength degradation model and generalised shear modulus degradation curves.

5 Geotechnical Soil Units

Interpretation of site-specific stratigraphy was performed by integrating geotechnical and geohazard core logging data with the AUV subbottom profiler (SBP) and 3D seismic geophysical data. This process involved (1) identifying general trends in the geotechnical data, (2) reviewing detailed geohazard core logging descriptions and then (3) integrating these data with the geophysical data to identify potential geophysical horizons. A geophysical horizon was mapped within the study area

Table 1 Geotechnical units across the site

Geotechnical unit	Generalised description	Geologic features
G1/G1a	Very soft to soft clay	Fine-grained stratified sediments (drapes)
G1b	Very soft to stiff clay	Fine-grained stratified sediments (drapes)
G2	Firm to stiff clay	Parallel-bedded, fine-grained sediments with the presence of localized mass transport deposits and/or channels
G3	Firm to stiff clay	Parallel-bedded, fine-grained sediments or fine-grained mass transport deposits
G4	Stiff clay	Parallel-bedded, fine-grained sediments or mass transport deposits
G5	Stiff to very stiff clay	Parallel-bedded, fine-grained sediments or mass transport deposits
G6	Very stiff to hard clay	Unit disrupted by numerous faults and characterised by chaotic seismic reflectors indicative of mass transport deposits

if it represented a significant geotechnical and/or geohazard core logging trend, unconformity, or other clear stratigraphic break, and it could be regionally mapped between different geotechnical exploration locations using available geophysical data. Five main horizons were identified across the study areas, dividing the shallow section into six geophysical units.

Geotechnical units which are systematic three-dimensional groupings of soils, with similar geotechnical properties and generally similar boundary elevations, were also defined for the study areas and shown in Table 1. Generally, good agreement was found between the geotechnical and geophysical units. The maximum depth of investigation across the site was 150 m below mudline (BML).

6 Index Properties

Although index properties including water content, plasticity index, liquidity index and submerged unit weight for the defined geotechnical units were generally consistent within each unit, there was, however, a large range of values within the units and in particularly in the surficial units. Furthermore, the depth dependency of soil parameter values was more obvious in the surficial units; for example, there was a clear depth-related increase in submerged unit weight in Unit G1a/G1, whereas in Units G2 to G6, depth-related increases were less obvious and so these units were treated as effectively independent of depth. In reality, a general increase in submerged unit weight would be expected, as there was a general trend of increasing strength with depth in all units and because increasing strength is nonlinearly related to a decrease in voids ratio (and a decreasing voids ratio leads to increasing submerged

Table 2 Characteristics of tested soils

Index property	Geotechnical unit	P15	P50	P85
Submerged unit weight	G1a/G1	4.0	4.8	5.7
	G1B	5.3	5.9	6.9
	G2	5.2	6.0	6.7
	G3	5.3	6.2	6.9
	G4	5.5	6.3	6.9
	G5	6.3	7.2	7.9
	G6	7.2	7.8	8.8
Plasticity index (PI) (%)	G1a/G1	53	63	75
	G1B	42	59	69
	G2	43	57	70
	G3	44	59	73
	G4	47	58	71
	G5	38	47	57
	G6	35	44	53
Specific gravity	All units	2.71	2.79	2.86

unit weight). This discrepancy highlights the important issue that geotechnical units are simplifications of observed soil properties to enable efficient geotechnical design.

The statistical P15, P50 and P85 values of the submerged unit weight, plasticity index and specific gravity for the defined geotechnical units are shown in Table 2, where P15, P50 and P85 are defined as the values below which lie 15%, 50% and 85% of the data values, respectively.

The organic contents of the soils encountered at the study site were generally between 1 and 10% with some values slighter higher than 13% at discrete depths suggesting the presence of localised organic matter from terrestrial plant fragments transported by streams offshore, or from marine phytoplankton. The carbonate contents were generally less than 10% with some local values up to 38% likely associated with localised occurrence of relatively high concentrations of foraminifera and/or shell fragments or occurrence of gassy soils and a platy/blocky structure in sediments. The soil salt content values were between 23 and 32 ppt which were lower than the global average of approximately, 35 ppt indicative of the marine deltaic origin.

7 Stress History and Consolidation Characteristics

Controlled-rate-of-strain (CRS), one-dimensional consolidation tests were performed on selected intact specimens recovered from the saved tube samples to evaluate the stress history of the soil formation across the whole study site.

Table 3 Statistical assessment of k_{ocr}

Location	P15	P50	P85
Site-wide facility locations	0.23	0.28	0.33

The preconsolidation pressures ($\sigma'_{v,m}$) were also estimated from the PCPT data, using the empirical correlation described in Lunne et al. (1997):

$$\mathrm{OCR} = k_{ocr}(q_{net}/\sigma'_{vo}) \tag{1}$$

where OCR is the over consolidation ratio and defined as the ratio of the maximum preconsolidation pressure and the present effective overburden stress. k_{ocr} is a correlation factor and q_{net} is a net piezocone resistance from PCPT. Typically, k_{ocr} is in a range of 0.2–0.5; higher values of k are recommended in aged heavily overconsolidated clays (Powell et al. 1988).

Statistical assessment of k_{ocr} across the whole study site based on sixty-three (63) good quality CRS test results was performed with the P15, P50 and P85 values given in Table 3. These values are within the range from Powell et al. (1988).

The soils across the study site comprised of underconsolidated soils (in situ vertical effective stress less than hydrostatic pressure with OCR < 1) and overconsolidated soils with OCR more than 4 as shown in Fig. 1 using methods proposed by Casagrande (1936) and Becker et al. (1987).

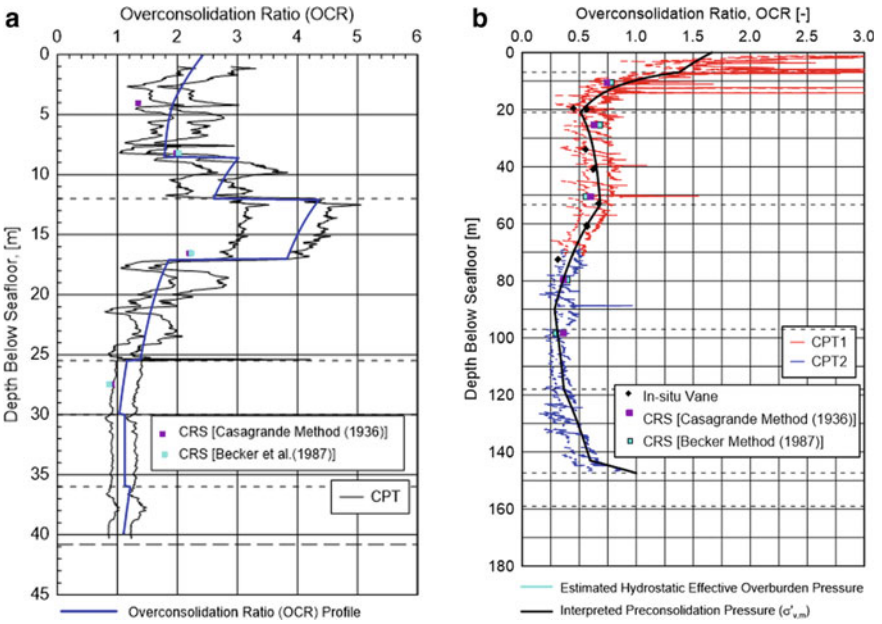

Fig. 1 **a** Example OCR profiles at the study site (OCR > 4). **b** Example OCR profiles at the study site (OCR < 4)

The coefficient of consolidation, c_v, was generally in the range of 0.6–6.4 m^2/year across the study site. c_v inferred from the remoulded CRS tests generally range between 0.4 and 1.0 m^2/year, which suggest that there are some soil fabric effects for the site and the excess pore pressures are expected to take longer to dissipate in remoulded soil than in intact soils.

Swelling index (c_s) describes the slope of the one-dimensional consolidation prior to preconsolidation pressure while compression index (c_c) defines the slope of virgin loading, i.e. post-preconsolidation pressure. c_c values between 0.3 and 1.5 were determined for intact specimens across the site and values between 0.5 and 0.7 were derived for remoulded specimens. c_s values were within the range of 0.03–0.15 for intact specimens with the ratio of c_s/c_c between 0.07 and 0.23.

8 Monotonic Undrained Shear Strength

The undrained shear strengths of the cohesive soils were evaluated by conventional laboratory strength tests (laboratory vane (LV), Fallcone, and UU triaxial compression tests), in situ PCPT, seabed T-bar and mini T-bar, and a suite of advanced static laboratory tests (static direct simple shear (CKoU′ DSS) and Ko-consolidated-undrained (CKoU) triaxial compression or extension tests). However, the T-bar, PCPT and advanced testing results are considered more reliable for assessing in situ conditions, due to concerns relating to the effect of unavoidable drilling disturbance on the index strength results.

The site-specific cone factor (N_{kt}) values can be developed from the PCPT net cone tip resistance (q_{net}) and the undrained shear strength (s_u). The advantage of using N_{kt} is that it normalises the data, thus effectively removing the depth dependency of the shear strength profile. Taking account of the fact that undrained shear strength is not an intrinsic measurement, separate assessments of N_{kt} as given in Table 4 were performed for UU triaxial, DSS and CKoU triaxial compression (CKoUC) and extension tests (CKoUE).

The derived N_{kt} values for the study site based on triaxial tests and DSS tests are comparable to those recommended by Andersen et al. (2008) as shown in Table 5.

An example plot of the interpreted intact shear strength profiles for a facility location is shown in Fig. 2. For this site, recommended characteristic trend lines of low estimate (LE) and high estimate (HE) UU triaxial shear strength s_{uu} interpreted from PCPT were provided as s_{uu} shear strength which is the reference shear strength for

Table 4 Statistical N_{kt} distribution

Test type	P15	P50	P85
DSS	11.4	13.2	15.1
UU	13.2	15.5	18.6
CKoUC	9.7	11.4	12.8
CKoUE	13.4	15.3	17.9

Table 5 Andersen et al. (2008)'s recommended N_{kt} values

Application	Based on $S_{u,CAUC}$[a]	Based on $S_{u,av}$ or $S_{u,DSS}$[a]
1. Overall, if limited previously experience	11.5 (9.5–13.5)	13 (11–15)
2. Gulf of Guineas	12.5 (10.5–14.5)	13.5 (11.5–15.5)
3. Norwegian Sea	11.5 (9.5–13.5)	14.5 (12.5–16.5)

[a]Mean (range)

ISO 19901-4 (2016) main text pile calculations. The interpreted DSS shear strength s_{ud} profile is also presented for suction pile design purpose.

Site-wide database of soil sensitivity S_t was generated by unit and on overall basis. The S_t statistics was developed based on intact and residual laboratory vane (M_v and $M_{v,re}$) values, intact and remoulded laboratory vane measurements (M_v and $M_{v,r}$), intact and remoulded UU triaxial test data and intact and remoulded fall cone test results. By the examination of the results for individual units, it was deemed reasonable to adopt the overall statistical values for all units. A sensitivity S_t value of 2.6 was generally adopted to derive LE and HE remoulded shear strength profiles. This value is comparable to the typical sensitivity S_t of Gulf of Mexico clays in the order of 2.5–3.0 (note that for Drammen clay, the sensitivity is typically in the range of 6–10). It should be noted, however, that site-specific adjustments to the remoulded shear strength profiles were occasionally deemed necessary particularly close to the unit boundaries.

9 Strain Rate Effects

The strain rate effects on the undrained shear strength were investigated by performing monotonic DSS tests at different shearing rates (0.6–85,493%/h). Figure 3 presents the measured undrained shear strengths normalised against the undrained shear strength from the corresponding tests conducted at the standard loading rate of ~5%/h, plotted as a function of strain rate and also plotted on Fig. 3 as background data for comparison purposes are the Drammen clay and other clay results published in Lunne and Andersen (2007). Although there is significant scatter in the range of measured results, the general trend of the test results is observed to be in reasonable agreement with the published data, but with a tendency to a slightly lower strain rate effect than for the other clays. A best-fit trend line through the test data is also shown in Fig. 3. The equations which define this trendline are as follows.

For strain rate (SR) $\geq$ 0.6%/h:

$$s_{ud\text{-}fast}/s_{ud} = 0.944\ SR^{0.0389} \quad (2)$$

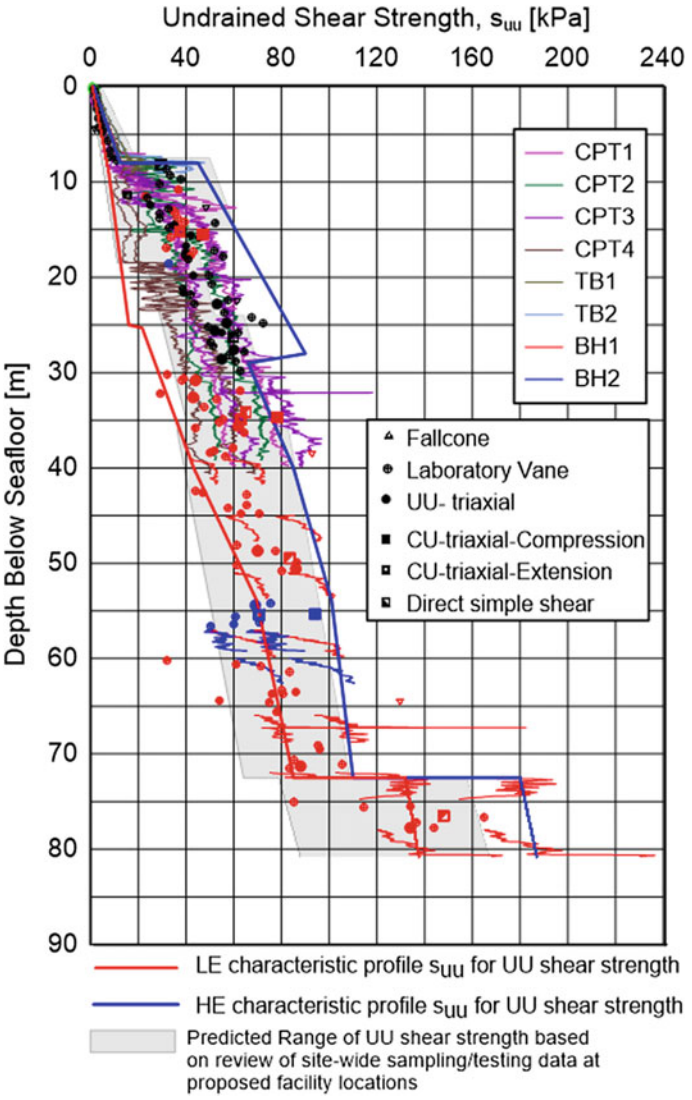

Fig. 2 Example intact shear strength profile for a facility location at the study site

For strain rate (SR) < 0.6%/h:

$$s_{\text{ud-fast}}/s_{\text{ud}} = 0.928\ \text{SR}^{0.0106} \tag{3}$$

where $s_{\text{ud-fast}}$ is the undrained shear strength measured from a test performed at a particular strain rate (note that in this equation $s_{\text{ud-fast}}$ can apply to strain rates higher or lower than the standard rate of 5%/h), s_{ud} is the undrained shear strength measured

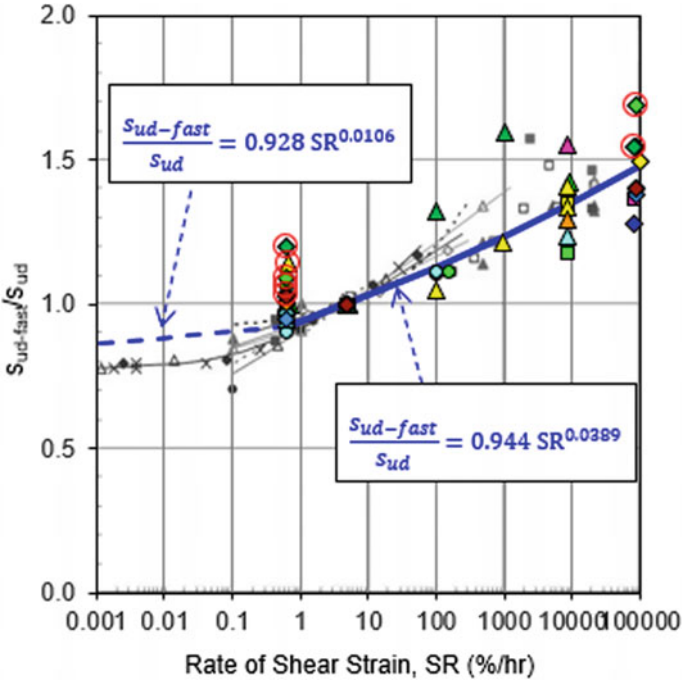

Fig. 3 Strain rate effects (background data in grey from Lunne and Andersen 2007). Unusual test results are circled and given less emphasis in fitting

from a test conducted at the standard loading rate of ~5%/h and SR is the strain rate (in % per hour).

For engineering design, the above relationship can be used to adjust the monotonic undrained shear strength profiles based on tests conducted at the standard strain rate of 5%/h, to the actual shear strain rate of interest for the problem under consideration. Although the strain rate effect has been specifically developed from simple shear data, the same equations and parameters can be adopted for assessing the strain rate effect for any other stress path.

10 Cyclic Undrained Shear Strength

10.1 Generalised Cyclic Strength Degradation Model

For engineering design at this development site, it was necessary to develop a generalised model which holistically considered all of this collected data, and from which an appropriate prediction of cyclic strength could be made for any element of soil, subject to any combination of cyclic loading and for any combination of monotonic

strength and in situ vertical effective stress. The cyclic response of the sediments was thoroughly investigated by conducting a large suite of cyclic DSS tests which was designed to test clusters of samples from different depths and reflecting a range of normalised shear strengths (s_{ud}/σ'_{vo}).

Classical S-N curves were constructed from individual sets of 2-way and 1-way test results, which enabled a site-specific generalised cyclic degradation model to be established for any combination of monotonic strength and in situ vertical effective stress in accordance with the following general expression:

$$s_{u\text{-}cyc}/s_{ud\text{-}fast} = a\exp(bs_{ud}/\sigma'_{vo}) + c < 1.0 \quad (4)$$

where a, b and c are empirical parameters.

For this study, trendlines for cyclic shear strains of 5, 10 and 15% each with $N =$ 5, 10, 15, 20 and 100 were fitted with the a, b and c parameters. An example of these parameters fitted with trendlines for $N = 10$ for 1-way and 2-way cyclic loading regimes are summarised in Tables 6 and 7 and shown in Fig. 4.

In Fig. 4, the ratio of cyclic undrained shear strength ($s_{u\text{-}cyc}$) to the monotonic undrained shear strength at the applicable cyclic loading rate ($s_{ud\text{-}fast}$) is presented as a function of s_{ud}/σ'_{vo} where s_{ud} is defined at the standard rate of shearing (5%/h). Although there is some scatter in the data, the fitted lines using Eq. (4) have been defined such that they closely follow the overall trends shown in the data, erring on the conservative side where there is any doubt. The form of Eq. (4) and ranges of appropriate values for the empirical parameters a, b and c are consistent with Fugro's extensive database of cyclic test results. This invariably indicates increasing degradation for higher normalised monotonic strengths (i.e. for higher s_{ud}/σ'_{vo}).

Table 6 Cyclic undrained shear strength parameters: 1-way, $N = 10$

Cyclic strain, γ_{cyc} (%)	Number of cycles, N	Empirical parameters		
		1-way strength		
		a	B	C
5	10	0.5	−7	0.63
10	10	0.5	−7	0.70
15	10	0.5	−7	0.76

Table 7 Cyclic undrained shear strength parameters: 2-way, $N = 10$

Cyclic strain, γ_{cyc} (%)	Number of cycles, N	Empirical parameters		
		2-way strength		
		a	b	c
5	10	0.4	−5	0.54
10	10	0.4	−5	0.60
15	10	0.4	−5	0.66

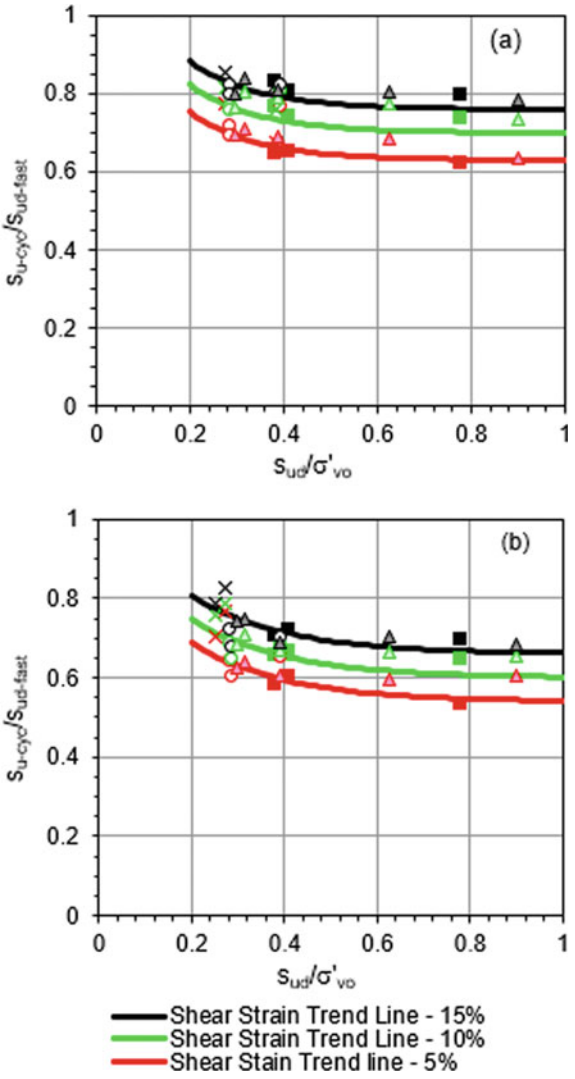

Fig. 4 **a** Cyclic strength 10 cycles 1-way, **b** cyclic strength 10 cycles 2-way

10.2 Failure Interaction Diagrams

In order to compare the predictions of the generalised cyclic strength degradation model presented in this study (based on tested material with a plasticity range of 34–81%) with existing clay models, such as Drammen Clay (Andersen 2004), failure interaction diagrams (FID) have been developed which present contours of the number of cycles to failure as a function of the average and cyclic shear stresses. An example of the comparison is present in Fig. 5 (original figure adopted from Andersen 2004) where $s_{ud}/\sigma'_{vo} = 0.25$ from this study is compared with OCR = 1

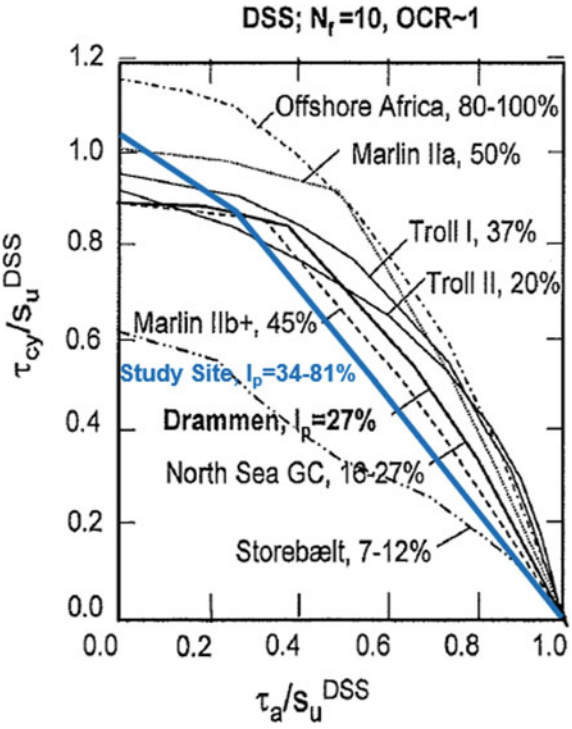

Fig. 5 Normalised shear stresses in simple shear causing failure after $N = 10$ for various clays (from Andersen 2004)

clays. Based on the DSS FID comparison shown in Fig. 5, the soils from this study appear to be more degradable than Drammen Clay and also more degradable than most of the presented clays under 1-way cyclic loads but is comparable or slightly less degradable under 2-way cyclic loads.

11 Shear Modulus and Shear Modulus Degradation

11.1 Shear Modulus and Cone Resistance Correlation

The maximum (or "small strain") shear modulus (G_{max}) was determined from a number of bender element and resonant column tests. The measured values of G_{max} are presented as a function of the corresponding cone resistance (q_c) on Fig. 6a. Also plotted in Fig. 6a, as background data and for comparison purpose, are other clay results published in Mayne and Rix (1993). As shown in this Fig. 6b, the site-specific test results are sensibly encompassed within the range of the published data. The site-specific measured G_{max} values are also plotted as a function of the corresponding net cone resistance (q_{net}) in Fig. 6b. Constant ratios for G_{max}/q_{net} of 20 and 50 were

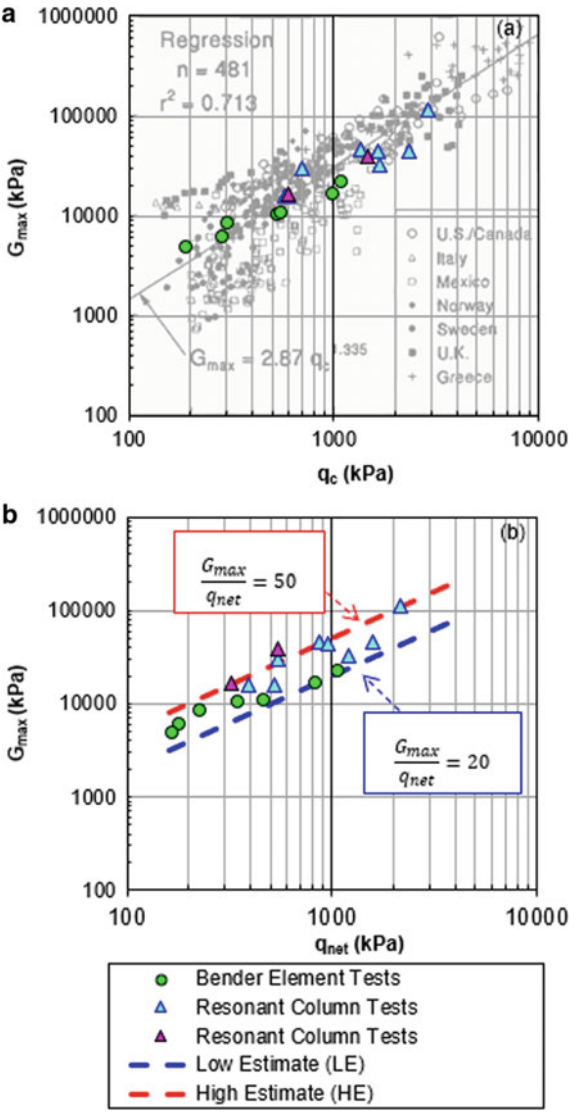

Fig. 6 **a** Comparison of test results with database of different clays (from Mayne and Rix 1993). **b** Correlation of maximum shear modulus and net cone resistance

proposed as the low estimate (LE) and high estimate (HE) design lines, respectively. As shown in Fig. 6b, the proposed relationship envelopes over 90% of the interpreted data. These design lines when combined with the appropriate q_{net} profiles can be used to derive the G_{max} profiles as input to assessing dynamic properties to use in seismic analysis.

11.2 Shear Modulus Degradation and Damping Ratio Curves

Analysis of nonlinear seismic ground response requires information on stiffness (shear modulus degradation) and material damping (damping curves) throughout the soil profiles at each location. In order to allow general application in a seismic analysis in a relatively simple way, the required seismic soil parameters for a range of soil conditions were developed using a generalised model pegged to the cone factor, N_{kt}. Having defined G_{max} as a fixed proportion of q_{net} (i.e. $G_{max}/q_{net} = 20$ or 50 for LE and HE stiffness, respectively) and since the undrained strength is also defined as a proportion of q_{net}, via the cone factor N_{kt}, for any fixed value of N_{kt}, there will be fixed values of G_{max}/s_{ud} (i.e. 20 N_{kt} for the LE G_{max} and 50 N_{kt} for the HE G_{max}). For each unique value of $G_{max}/s_{ud,}$ a single stress–strain curve can be derived that encompasses the full response from small to large strain. However, since G_{max}/s_{ud} varies with different values of N_{kt} separate stress–strain relationships must be defined for each potential value of N_{kt}.

Accordingly, modulus reduction curves (G/G_{max}) for seismic design were developed and are presented in Fig. 7 for different values of N_{kt} (covering the range found at the site) and for the proposed LE and HE G_{max}/q_{net} ratios and also shown in Fig. 7 are the results from the resonant column tests. In terms of G/G_{max}, it can be seen that the recommended design curves sensibly encompass the range of measured data, particularly for the most common range of expected N_{kt} values.

The damping ratio (D) defines the energy dissipated by the soil and is generally assessed based on the soil stress–strain hysteresis loops. The stress–strain hysteresis loops are defined using two functions: one describing the "backbone curve" and the other describing the "unload/ reload" behaviour. In this study, the backbone curve was defined using the relationship between τ and γ obtained from the generalised stress–strain curves from the DSS results. The "unload/ reload" behaviour was modelled using the Masing rule (Pyke 1979), since this is the most common assumption built into nonlinear site response analysis software. The resulting damping ratio curves are presented in Fig. 8, and it may be noted that the recommended design curves typically slightly underpredict the measured damping ratio for very low strains (γ less than about 0.05%), but thereafter generally provide a sensible fit up to the limit of the resonant column data (γ about 0.4%). At larger strains, it is commonly found that Masing rule-based models tend to overestimate the actual damping ratio, as has been previously reported in the literature (e.g. Lo Presti et al. 2006). For engineering design, alternative strategies such as using engineering models that do not employ the Masing rule or utilising a reduced or equivalent shear modulus (Yamamoto et al. 2015) may be adopted.

For seismic analysis conducted using a simplified equivalent linear approach (e.g. SHAKE), the damping ratio can be defined independently of the shear modulus degradation curves, and in such software adopting the damping response recommended by Vucetic and Dobry (1991), for plasticity index of 50% may be appropriate. This relationship is also shown in Fig. 8.

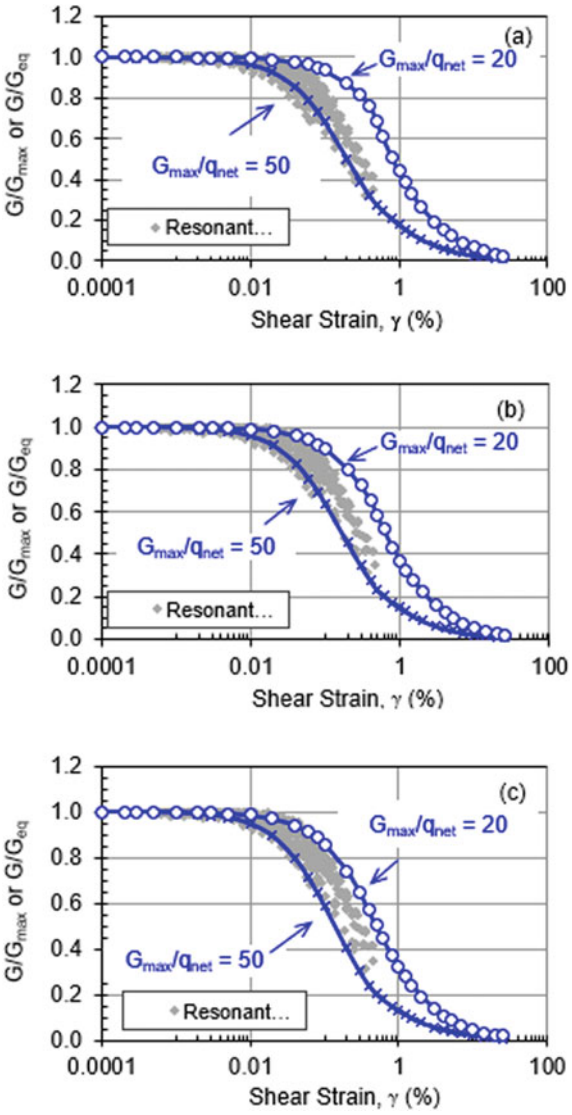

Fig. 7 Shear modulus degradation curves cone factors, **a** $N_{kt} = 11$, **b** $N_{kt} = 13$ and **c** $N_{kt} = 15$

12 Conclusion

This paper presented key results from a recent offshore geotechnical site investigation and subsequent comprehensive onshore laboratory testing and interpretation carried out for an offshore development in the Krishna Godavari (KG) Basin, Bay of Bengal. The interpretation was carried out using a consistent framework leveraging site-wide data to characterise the recovered sediments. The undrained shear strength, shearing

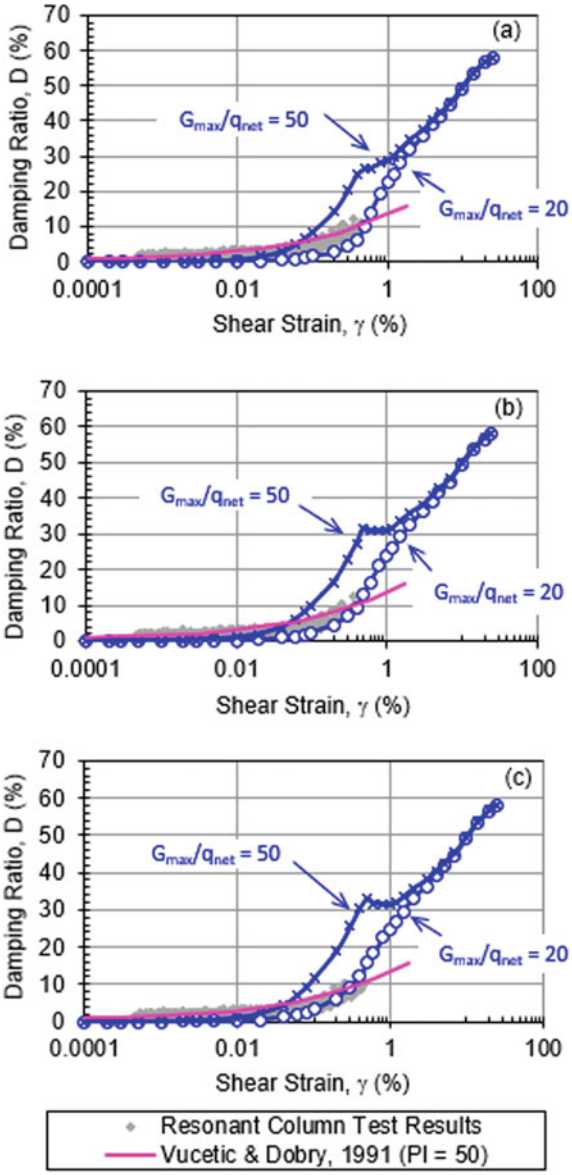

Fig. 8 Damping ratio curves, **a** cone factors, $N_{kt} = 11$, **b** cone factors, $N_{kt} = 13$ and **c** cone factors, $N_{kt} = 15$

rate effect and the cyclic and seismic behaviours of the range of materials recovered across the site are found to be different but comparable to other clays in the literature.

References

Andersen KH (2004) Cyclic clay data for foundation design of structures subjected to wave loading. In: International conference on cyclic behaviour of soils and liquefaction phenomena, CBS04, Bochum

Andersen KH, Lunne T, Kvalstad TJ, Forsberg CF (2008) Deep water geotechnical engineering. In: Proceedings of XXIV national conference of Mexican society of soil mechanics, Aguascalientes, 26–29 Nov 2008

Becker DE, Crooks JHA, Been K, Jefferies MG (1987) Work as a criterion for determining in situ and yield stresses in clays. Can Geotech J 24:549–564

Casagrande A (1936) Determination of the preconsolidation load and its practical significance. In: Proceedings, first international conference on soil mechanics and foundation engineering, vol 3, Cambridge, pp 60–64

ISO 19901-4 (2016) Petroleum and natural gas industries—specific requirements for offshore structures—part 4: geotechnical and foundation design considerations, 2nd edn

Lo Presti DC et al (2006) ONDA: computer cone for nonlinear seismic response analyses of soil deposits. J Geotech Geoenviron Eng ASCE 132(2):223–236

Lunne T, Andersen KH (2007) Soft clay shear strength parameters for deepwater geotechnical design. In: Proceedings of the 6th OSIG, London, pp 151–176

Lunne T, Robertson PK, Powell JJM (1997) Cone penetration testing in geotechnical practices. Blakie Academic Professional, New York

Mayne PW, Rix GJ (1993) G_{max}-qc relationships for clays. Geotech Test J GTJODJ 16(1):54–60

Powell JJM, Quaterman RST, Lunne T (1988) Interpretation and use of the piezocone test in UK clays. In: Proceedings of penetration testing in the UK, London, pp 151–156

Pyke R (1979) Non-linear soil models for irregular cyclic loading. J Geotech Eng ASCE 105(GT6):715–726

Rao NK, Saito Y, Nagakumar KCV, Demudu G, Rajawat AS, Kudo S, Li Z (2015) Palaeogeography and evolution of the Godavari delta, east coast of India during the Holocene: an example wave-dominated and fan-delta settings. Palaeoogeogr Palaeoclimatol Palaeoecol 440:67–74

Vucetic M, Dobry R (1991) Effect of soil plasticity on cyclic response. J Geotech Eng Div ASCE 117(1):89–107

Yamamoto N, Sharma S, Erbrich CT (2015) Suitability of Masing rules for seismic analysis of offshore carbonate sediments. In: Frontiers in offshore geotechnics, ISFOG 2015, Oslo, 10–12 June 2015